

Quantitative Physiology of the Precancerous Cervix *In Vivo* through Optical Spectroscopy¹

Vivide Tuan-Chyan Chang^{*}, Peter S. Cartwright[†], Sarah M. Bean[‡], Greg M. Palmer[§], Rex C. Bentley[‡] and Nirmala Ramanujam^{*}

^{*}Department of Biomedical Engineering, Duke University, 136 Hudson Hall, Durham, NC 27708, USA; [†]Department of Obstetrics and Gynecology, Duke University School of Medicine, Box 3084, Durham, NC 27710, USA; [‡]Department of Pathology, Duke University School of Medicine, Box 3712, Durham, NC 27710, USA; [§]Department of Radiation Oncology, Duke University School of Medicine, Box 2082, Durham, NC 27710, USA

Abstract

Cervical cancer is the second most common female cancer worldwide. The ability to quantify physiological and morphological changes in the cervix is not only useful in the diagnosis of cervical precancers but also important in aiding the design of cost-effective detection systems for use in developing countries that lack well-established screening and diagnostic programs. We assessed the capability of a diffuse reflectance spectroscopy technique to identify contrasts in optical biomarkers that vary with different grades of cervical intraepithelial neoplasia (CIN) from normal cervical tissues. The technology consists of an optical probe and an instrument (with broadband light source, dispersive element, and detector), and a Monte Carlo algorithm to extract optical biomarker contributions including total hemoglobin (Hb) concentration, Hb saturation, and reduced scattering coefficient from the measured spectra. Among 38 patients and 89 sites examined, 46 squamous normal sites, 18 CIN 1, and 15 CIN 2⁺ sites were included in the analysis. Total Hb was statistically higher in CIN 2⁺ ($18.3 \pm 3.6 \mu\text{M}$, mean \pm SE) compared with normal ($9.58 \pm 1.91 \mu\text{M}$) and CIN 1 ($12.8 \pm 2.6 \mu\text{M}$), whereas scattering was significantly reduced in CIN 1 ($8.3 \pm 0.8 \text{ cm}^{-1}$) and CIN 2⁺ ($8.6 \pm 1.0 \text{ cm}^{-1}$) compared with normal ($10.2 \pm 1.1 \text{ cm}^{-1}$). Hemoglobin saturation was not significantly altered in CIN 2⁺ compared with normal and CIN 1. The difference in total Hb is likely because of stromal angiogenesis, whereas decreased scattering can be attributed to breakdown of collagen network in the cervical stroma.

Neoplasia (2009) 11, 325–332

Introduction

Carcinoma, accounting for more than 70% of all cancers in the United States today [1], arises from tissue of epithelial origin. Examples of squamous epithelial carcinomas include those of the cervix, skin, and oral cavity.

Since the introduction of the Papanicolaou test in the United States, both the incidence and the mortality rates of cervical cancer have decreased to 8.4 per 100,000 and 2.5 per 100,000 women, respectively [1,2]. This success has been attributed to cytology screening programs paired with colposcopic-based diagnosis and treatment programs. Colposcopy, a visual examination of the cervix under magnification followed by biopsy of the suspicious lesion, classifies cervical cells into normal, low-grade cervical intraepithelial lesion (CIN 1),

high-grade cervical intraepithelial lesion (CIN 2 or CIN 3), and/or invasive cancer. Colposcopy has excellent sensitivity (>90%); however,

Abbreviations: CIN, cervical intraepithelial neoplasia; CIN 2⁺, high-grade CIN; Hb, hemoglobin; oxyHb, oxygenated hemoglobin; deoxyHb, deoxygenated hemoglobin; λ , optical wavelength; $\mu_a(\lambda)$, optical absorption coefficient as a function of wavelength; $\mu_s'(\lambda)$, optical reduced scattering coefficient as a function of wavelength

Address all correspondence to: Nirmala Ramanujam, PhD, 136 Hudson Hall, Durham, NC 27708. E-mail: nimmi@duke.edu

¹Funding support was provided by the National Institutes of Health grant R21-CA108490-01.

Received 28 October 2008; Revised 14 January 2009; Accepted 16 January 2009

Copyright © 2009 Neoplasia Press, Inc. All rights reserved 1522-8002/09/\$25.00
DOI 10.1593/neo.81386

its specificity is poor (<50%) even in the hands of expert colposcopists, hence often leading to needless biopsies [3,4]. The introduction of the human papillomavirus (HPV) vaccine is not likely to obviate the need for the need for colposcopy, particularly for women already infected with HPV or for whom the vaccine is prohibitively expensive.

Among women worldwide, cervical cancer is the second most common cancer with an incidence rate of 16.2 per 100,000 and a mortality rate of 9 per 100,000 women [2,5]. This is largely attributed to the fact that many countries do not have the appropriate infrastructure and resources to support the organized screening and diagnostic programs that are available to women in the United States. There is a critical need for low-cost, time-saving, and effective approaches to diagnose cervical cancer in the worldwide population. The constraints of cytology-based screening in low-resource settings have prompted the evaluation of alternative methods including visual inspection after application of acetic acid and iodine solution with the unaided eyes, at low magnification, or with a digital camera [6,7]. However, even in highly controlled research environments, the sensitivity and specificity of these visualization-based screening techniques are 0.77 and 0.65 [8], respectively, which is highly unlikely to be reproduced in routine service settings within an underresourced community.

Optical technologies, particularly diffuse reflectance spectroscopy, present a potentially affordable approach for fast, noninvasive, and accurate detection of cervical cancer. Diffuse reflectance spectroscopy is a technique that is sensitive to the absorption and scattering properties of tissues. In the near UV and visible wavelengths, dominant absorbers in the cervix are oxygenated (oxyHb) and deoxygenated hemoglobin (deoxyHb), arising from blood vessels in the stroma. Scattering primarily arises from cell nuclei and organelles (epithelium and stroma), as well as collagen fibers and cross-links (stroma). Neoplastic tissue exhibits significant changes in their optical signature. Stromal absorption generally increases with angiogenesis and increased microvessel density, whereas epithelial scattering increases due to increased cytoplasm-to-nuclear ratio and hyperchromasia [9–11]. Stromal scattering, conversely, has been shown to decrease with neoplastic progression as extracellular collagen network breaks down [10,12].

UV-visible reflectance spectroscopy has been successfully developed as a diagnostic tool for precancers and cancers in the uterine cervix [10,13–20], breast [21–23], gastrointestinal tract [24–26], to name just a few examples. Several preclinical and clinical systems for cervical cancer diagnosis are available [18,27–30] to serve an adjunct role to improve the sensitivity and specificity of colposcopy [28]. Previously developed techniques have primarily relied on pattern recognition of the measured spectra to extract features for classification, and thus do not directly contribute to the understanding of underlying morphological and biochemical changes that occur in the precancerous cervix *in vivo* [9–12]. Understanding the underlying sources of contrast in the precancerous cervix will hone in on the features of the reflectance spectra that are best able to discriminate between precancerous and normal tissues. Having this knowledge should enable the construction of more inexpensive diagnostic systems that may be used in communities where the infrastructure for well-organized screening and diagnostic programs is lacking.

A number of recent studies have developed mathematical models and methods to quantify the absorption and scattering properties of the cervix from reflectance measurements. Georgakoudi et al. [15] observed a trend toward smaller and flatter reduced scattering spectrum ($\mu_s'(\lambda)$) in the cervix using UV-visible reflectance spectroscopy coupled with a diffusion equation-based mathematical

model. Collier et al. [31] quantified an increase in scattering of the cervical epithelium using Beer's law-based analysis of near infrared (NIR) confocal microscopy results. Georgakoudi et al. [11] also used light scattering spectroscopy from 350 to 700 nm and found an increase in nuclear density with CIN compared with normal tissue *in vivo*. Mourant et al. [32] used polarized light scattering from 500 to 1000 nm to quantify Hb concentration and saturation and found that the slopes and ratios were the most diagnostically useful in distinguishing CIN 2⁺ from non-CIN 2⁺. Mourant et al. did not see a significant difference in total Hb and Hb saturation between CIN 2⁺ from normal and CIN 1 when colposcopically normal sites are included. Hornung et al. [16] quantified cervical scattering and Hb concentration using diffuse reflectance spectroscopy at select NIR wavelengths and a diffusion-based model *in vivo*. In the same study, Hornung et al. found that [oxyHb] decreased in CIN 2⁺ compared with normal, whereas [deoxyHb] was statistically indistinguishable. Scattering also decreased at certain wavelengths from normal to CIN 2⁺. These studies demonstrated that precancerous cervical tissue can be distinguished from normal tissue based on optical biomarkers derived from the absorption and scattering properties of tissue *in vivo*.

The study presented in this paper builds on the excellent body of work on the quantification of optical biomarkers in cervical neoplasia. We have developed an optical toolbox consisting of a fiber-optic-based spectrometer and a stochastic model based on a Monte Carlo algorithm [33] to quantify rapidly and nondestructively *in vivo* the absorption and scattering properties of tissues from diffuse reflectance spectra measurements. The primary difference between the clinical systems described above for diffuse reflectance spectroscopy and our technology is the mathematical approach used to quantify the underlying sources of intrinsic contrast. The mathematical model we have developed is applicable over a wide wavelength range (UV-visible) for which the diffusion equation is not well suited and the physical illumination and collection geometry of the optical probe can be accurately accounted for in the model. We conducted a pilot clinical study to quantify the absorption and scattering properties of normal, low-grade, and high-grade precancers of the human cervix *in vivo* using our technology and identified the biomarkers that showed the statistically most significant differences between high-grade precancers and all other tissue types. We also compared the results of our study to those previously reported [11,16,31] to compare the conclusions reached using different approaches in the clinic. In addition, we compared the trend reported in our study for total Hb concentration to the microvessel density analysis of the cervix reported in the literature [12,34–38].

Methods

Clinical Study

Protocol design The study protocol was reviewed and approved by the Institutional Review Board at Duke University Medical Center. Patients referred to the Duke University Medical Center Colposcopy Clinic after an abnormal Papanicolaou test result were recruited for the study. Pregnant women were excluded from study. Diffuse reflectance, delivered to and collected through a fiber-optic probe, was collected from one to three visually abnormal site(s) immediately after colposcopic examination of the cervix with the application of 5% acetic acid. This was followed by an optical measurement on a

colposcopically normal site from the same patient. Optical interrogation of colposcopically normal and abnormal sites was conducted before biopsy to avoid confounding absorption due to superficial bleeding. Biopsy samples were taken only from colposcopically abnormal sites. Identification of abnormal site, placement of the probe on the cervix, and biopsies were made by the same gynecologist (P.S.C.). Initially, probe motion during data collection was an issue, but this was later addressed with a custom-designed probe holder by Duke Physics Machine Shop, constructed out of Delrin to withstand sterilization. The probe holder secured the probe onto the speculum, reducing patient and probe motion artifact. Optical data were correlated with the adjudicated biopsy diagnoses (S.M.B. and R.C.B.).

Instrumentation

Spectrometers Two spectrometers were used for this clinical study: a custom-built spectrometer (Instrument A) and SkinScan (Instrument B), both from JY Horiba (Edison, NJ). The spectrometers and fiber-optic probe (Figure 1) have been described in detail in previously published studies [39,40]. Briefly, the illumination component of Instrument A has a 450-W Xe arc lamp and double-grating monochromator (1200 grooves per millimeter grating), and its detection module consists of an imaging spectrograph (300 grooves per millimeter grating) and CCD camera for simultaneous wavelength detection. The illumination arm of Instrument B consists of a 150-W Xe arc lamp and a double-grating monochromator (1200 grooves per millimeter grating), and the detection arm consists of a monochromator (1200 grooves per millimeter grating) and a photomultiplier, which detects the intensity one wavelength at a time. The grating of the monochromator in Instrument A was set to zeroth order for broadband (white) light illumination. Integration time was set to 100 milliseconds for both instruments. Because Instrument A is capable of detecting all wavelengths simultaneously, one diffuse reflectance spectrum measurement took approximately 200 milliseconds, whereas the same measurement took approximately 3 seconds on Instrument B. The spectral resolutions were 10 and 3.5 nm for Instruments A and B, respectively. Both instruments were wavelength-calibrated at the beginning of the day by measuring the peak position of a HeNe laser (Instrument A) or Si photodiode (Instrument B). To account for the wavelength-dependent throughput of the system and drifts in lamp intensity, the raw diffuse reflectance spectrum was calibrated through division by reflectance from a reflectance standard (Spectralon; LabSphere, North Sutton, NH). The measured reflectance spectrum from 450 to 600 nm was interpolated at 5-nm intervals using a cubic spline function (MATLAB; Mathworks, Natick,

MA). Data where the gynecologist noted probe motion or significant patient motion were excluded from data analysis. Two sites were rejected for probe motion before the use of the probe holder, compared with one rejected site afterward.

Fiber-optic probe A bifurcated fiber-optic probe (RoMack, Williamsburg, VA) was used to collect diffuse reflectance from patients recruited for the study. The common end (that is in contact with tissue) consists of a central bundle of 19 illumination fibers, encircled by a ring of 18 collection fibers (Figure 1). All fibers are multimode (200/240- μm core/cladding diameter) and have a numerical aperture of 0.22. The fibers are epoxied inside a stainless steel tube with an outer diameter of 3.2 mm. The stainless steel tube was sterilized in Cidex OPA (ASP, Irving, CA) for 20 minutes before each procedure for disinfection.

The sensing depth of the fiber-optic probe, defined as the maximum depth that 50% to 90% of the detected photons ever penetrated, was evaluated using Monte Carlo simulations similar to [40,41]. Monte Carlo modeling is a numerical technique that is valid for a wide range of tissue properties and can be used to model light transport in biological tissue over the entire UV-VIS-NIR wavelengths [33,42]. A Monte Carlo code [41] was used to carry out diffuse reflectance simulations on a two-layered tissue model using absorption and scattering coefficients of the cervical epithelium and stroma reported by Chang et al. [43,44]. On the basis of the definition provided above, the mean sensing depth for λ between 450 and 600 nm was 523 and 1070 μm up to 50% and 90%, respectively. Because the average thickness of cervical epithelium varies between 200 and 350 μm [43–45], photons collected by the probe contain information from both epithelial and stromal layers, with increasing stromal contribution as the wavelength increases. Epithelial thickness does not seem to correlate with pathology, although it is dependent on age and decreases in postmenopausal women [44].

Pathology (consensus reading) Colposcopic biopsies were fixed in 10% buffered formalin, embedded in paraffin, sectioned, and stained with hematoxylin and eosin per routine protocols. Original histological diagnoses were rendered by four board-certified anatomic pathologists with expertise in gynecologic pathology. Original biopsy slides were blindly reviewed again (S.M.B.). When a diagnostic discrepancy occurred on review, a second pathologist (R.C.B.) examined the case. The second pathologist's diagnosis served as the tiebreaker. For biopsies where three-way disagreement occurred, the two reviewing pathologists examined the cases concurrently at a multiobserver microscope to establish a consensus diagnosis. Diagnoses were based on the World Health Organization classification of HPV-associated intraepithelial lesions of the cervix (CIN) [46,47] and included the following: negative for dysplasia, HPV cytopathic effect/CIN 1, CIN 2, and CIN 3. Pathologists often find it difficult to distinguish between CIN 2 and CIN 3; hence, both are often lumped together as high-grade intraepithelial lesion (CIN 2⁺). Epidemiologically, CIN 2⁺ are more likely to progress to invasive carcinoma as compared with low-grade lesions, which commonly spontaneously regress [48]. Hence, methods to reliably distinguish between normal and CIN 1 *versus* CIN 2⁺ are desirable.

Data Analysis and Validation

A flexible and fast Monte Carlo-based inverse model developed previously by our group [33] was used to extract the absorption and

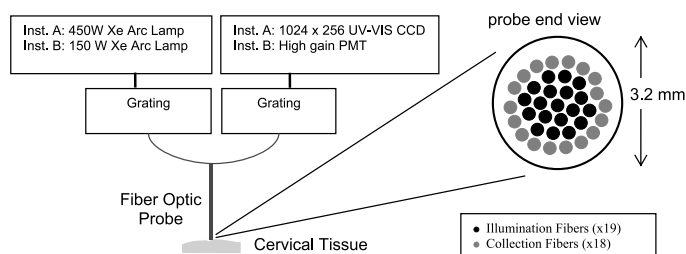


Figure 1. A schematic of the fiber-optic-based spectrometer. Currently, the system is housed on a mobile cart in the colposcopy clinic.

scattering properties of the cervical tissue from the measured diffuse reflectance spectra. The model is valid for a wide range of optical properties and easily adapts to any probe geometry provided a one-time calibration is performed on a synthetic phantom with known absorption and scattering coefficients. The wavelength-dependent extinction coefficients for the absorber and refractive indices of the scatterer and surrounding medium are considered fixed parameters in the inverse model [33]. The average refractive indices over 450 to 600 nm used in the model for the scatterer and the surrounding medium, water, are 1.60 and 1.34, respectively [33]. The wavelength-dependent extinction profile of oxyHb and deoxyHb are reported by Prahl [49]. The free parameters that are iteratively searched during fitting include absorber concentration, scatterer size, and volume density of scatters. A Gauss-Newton nonlinear least-squares optimization algorithm (MATLAB; Mathworks) was used to minimize the difference between the measured and the Monte Carlo-simulated diffuse reflectance [33]. A ratio of the measured reference phantom reflectance to the modeled reference phantom reflectance gives a calibration factor that enables a direct comparison between measured and predicted reflectance spectra during the inversion process. This model has been extensively validated [33,50] and used by our group in a number of preclinical and clinical studies [23,40,50–55].

Validation on synthetic tissue phantoms A total of 10 phantoms (for each instrument) with tissue-mimicking optical properties were constructed to study the accuracy with which absorption and scattering over the 450- to 600-nm wavelength range can be quantified. Details of the validation can be found in Bender et al. [50]. Briefly, phantoms were constructed from a homogenized suspension (using magnetic stirrers) of monodisperse polystyrene scatters (1- μm diameter polystyrene spheres, catalog no. 07310; Polysciences, Warrington, PA) and human Hb absorbers (H0267 ferrous stabilized human Hb; Sigma-Aldrich, St. Louis, MO). Table 1 shows the ranges and means of the absorption $\mu_a(\lambda)$ and scattering coefficients $\mu_s'(\lambda)$ of these phantoms over the 450- to 600-nm wavelength range. A range of optical properties is reported because values are wavelength-dependent. The optical properties are chosen based on previously reported literature values [43,50]. The expected values for $\mu_a(\lambda)$ were determined using a spectrophotometer and Beer's law, whereas $\mu_s'(\lambda)$ of the phantoms were computed using Mie theory.

Data Processing

Raw diffuse reflectance was calibrated by dividing the reflectance from a reflectance standard, and then input into the inverse model to extract $\mu_s'(\lambda)$, $\mu_a(\lambda)$, and the concentrations of endogenous ab-

sorbers, oxyHb and deoxyHb. For clinical data analysis, phantom 9 was chosen as the reference phantom based on recommendations from Bender et al. [50]. A medium-scattering phantom with clinically relevant concentration of Hb enables flexible and accurate inversion of clinical data using the Monte Carlo model.

Results

Phantom Validation

Diffuse reflectance was collected on identically structured phantom sets using both Instruments A and B. Details of the validation can be found in Bender et al. [50]. Using Instrument A, percent extraction errors for mean μ_a , [Hb], and mean μ_s' were $7.0 \pm 9.4\%$, $6.0 \pm 6.7\%$, and $7.6 \pm 5.9\%$ (mean \pm SD), respectively. Using Instrument B, percent extraction errors for mean μ_a , [Hb], and mean μ_s' were $5.5 \pm 3.4\%$, $3.7 \pm 4.2\%$, and $2.4 \pm 1.8\%$, respectively. Standard deviation was calculated using different reference phantoms.

Patients and Biopsy Results

A total of 89 sites were optically interrogated in 38 female patients aged 18 to 34 years (mean \pm SD, 24.7 ± 4.4 years). All recruited patients were premenopausal. Ten sites were excluded secondary to motion artifact ($n = 3$), other tissue types ($n = 5$), and ungradable biopsies ($n = 2$). Consensus reading results of the sites are listed in Table 2. No invasive squamous cell carcinoma or glandular lesions were identified in this cohort.

Clinical Study

Figure 2A depicts calibrated diffuse reflectance derived from a colposcopically normal site, as well as biopsy-proven CIN 1 and CIN 2⁺ sites from the same patient.

Diffuse reflectance from normal cervical sites is higher than those from dysplastic tissue owing to increased absorption and decreased scattering in dysplastic tissue. Troughs in the calibrated diffuse reflectance spectrum represent wavelengths where there are strong absorptions. The α and β absorption peaks of oxyHb are visible near 542 and 576 nm in normal, CIN 1 and CIN 2⁺ sites. Figure 2, B and C, shows the extracted absorption and reduced scattering spectra extracted from the same patient for different types of tissue. The extracted absorption spectra closely match the absorption spectrum of oxyHb with the α and β absorption peaks of oxyHb. The extracted reduced scattering spectra (Figure 2C) are fairly featureless and monotonically decrease over the measured wavelength range. Absorption, and hence, the total Hb concentration, increases, whereas scattering decreases as tissue progresses from normal to CIN 1 and then to CIN 2⁺.

Table 1. Phantom Hemoglobin (Hb) Concentration, Mean, Minimum, and Maximum Absorption $\mu_a(\lambda)$ and Reduced Scattering $\mu_s'(\lambda)$ Coefficients (450-600 nm).

Phantom No.	[Hb] (μM)	Mean μ_a (cm^{-1})	Min μ_a (cm^{-1})	Max μ_a (cm^{-1})	Mean μ_s' (cm^{-1})	Min μ_s' (cm^{-1})	Max μ_s' (cm^{-1})
1	5.70	0.42	0.05	0.75	25.94	23.55	28.50
2	6.11	0.45	0.06	0.80	21.59	19.61	23.73
3	6.51	0.48	0.06	0.86	17.28	15.68	18.98
4	6.93	0.51	0.07	0.91	12.95	11.76	14.23
5	9.85	0.74	0.14	1.28	11.32	10.28	12.44
6	9.85	0.74	0.14	1.28	18.93	17.19	20.80
7	10.12	0.74	0.10	1.33	25.94	23.55	28.50
8	10.85	0.79	0.10	1.42	21.59	19.61	23.73
9	11.57	0.85	0.11	1.52	17.28	15.68	18.98
10	11.97	0.92	0.17	1.59	18.54	16.84	20.37

Table 2. Pathology Consensus Reading Result.

Total (89)	Included (79)				Excluded
	Normal Squamous		Precancerous Squamous		
	Colposcopically Normal (Not a Biopsy Sample)	Biopsy-Confirmed Normal (Colposcopically Abnormal)	CIN 1	CIN 2 ⁺	
Number of sites	34	12	18	15	10*

*Excluded data include normal columnar ($n = 4$), motion ($n = 3$, of which 2 were before the use of probe holder), ungradable biopsies ($n = 2$), and flat condyloma ($n = 1$). Motion was noted when the gynecologist noted a drift in the probe before and after light interrogation. Normal columnar tissues were excluded from the analysis because of the small sample size.

Statistical Analysis

Kruskal-Wallis tests were used to assess global differences in the extracted parameters among different tissue grades, and *post hoc* Wilcoxon rank sum tests were performed using diffuse reflectance from 450 to 600 nm when the global test is significant at the $P < .05$ level. In identifying different combinations of tissue grades showing differential measurements, we have incorporated the Bonferroni correction for the multiple *post hoc* tests. Because CIN 1 are often symptomatic of viral infection and inflammation and regress to normal tissue over time, the clinical emphasis is on distinguishing between CIN 2⁺ from normal and CIN 1 tissues [48]. A summary of extracted optical and physiological parameters and the results of statistical tests can be found in Table 3.

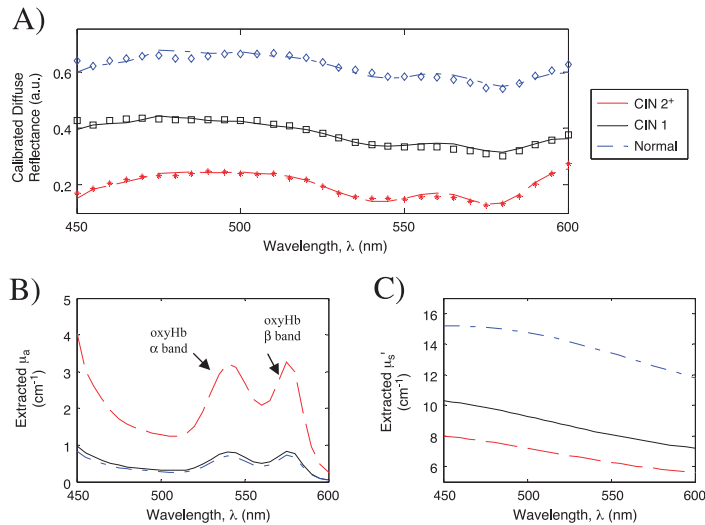


Figure 2. (A) Typical fits of calibrated diffuse reflectance (450-600 nm) from a normal site (blue diamonds), a CIN 1 site (black squares), and a CIN 2⁺ site (red asterisks) of the same patient. Dashed lines are fits to the measured diffuse reflectance data (100 fits) using the Monte Carlo-based inverse model. Diffuse reflectance from a CIN 2⁺ site has lower reflectance due to higher absorption and lower scattering. The CIN 1 site has intermediate scattering and absorption. (B) Extracted absorption spectrum ($\mu_a(\lambda)$) from a normal site (blue diamonds), a CIN 1 site (black squares), and a CIN 2⁺ site (red asterisks) from the same patient. Absorption is significantly increased in CIN 2⁺ compared with normal cervical tissue and CIN 1. (C) Extracted reduced scattering spectrum ($\mu_s'(\lambda)$) from a normal site (blue shaded line), a CIN 1 site (black squares), and a CIN 2⁺ site (red broken line) from the same patient. Scattering decreases from normal cervical tissue to CIN 1 and decreases further from CIN 1 to CIN 2⁺. Scattering spectrum is fairly featureless and monotonically decreases from 450 to 600 nm.

Figure 3 shows box and whisker plots of total Hb concentration and the wavelength-averaged reduced scattering coefficient of all tissue types. The *middle line* represents the median, the *upper and lower edges* represent the 75th and 25th percentiles, respectively, and *crosses* indicate outliers. Combining normal and CIN 1, [total Hb] increased significantly in CIN 2⁺ compared with normal and CIN 1 ($P < .002$). [Total Hb] is also statistically increased in CIN compared with normal cervical tissue ($P < .023$). Mean reduced scattering ($\langle \mu_s'(\lambda) \rangle$) from 450 to 600 nm is significantly decreased as tissue progresses from normal to CIN ($P < .002$). The directions of changes in [Total Hb] and $\langle \mu_s'(\lambda) \rangle$ were preserved when only biopsy-confirmed normal sites were used, but no statistically significant differences were observed ($P < .06$ and $P < .41$ for [total Hb] and $\langle \mu_s'(\lambda) \rangle$ in CIN 2⁺ vs normal and CIN 1, respectively). This is likely because of the small number of biopsy-confirmed normal sites ($n = 12$) compared with the number of colposcopically normal sites ($n = 36$).

Discussion

Diffuse reflectance spectroscopy has been used to identify cervical precancers and multiple commercialization efforts are underway

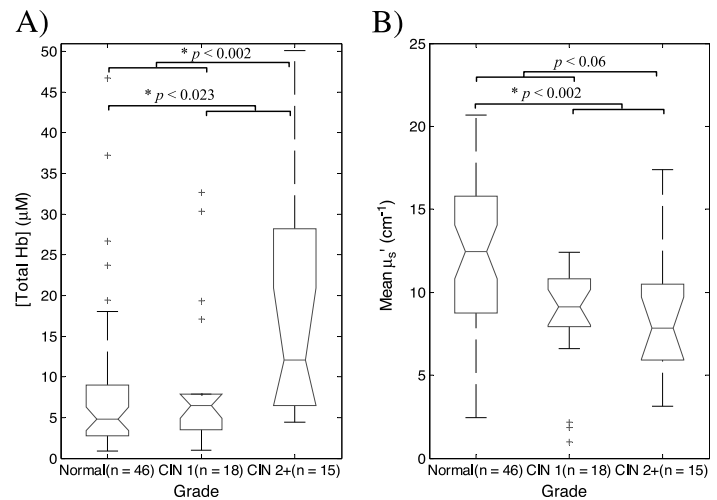


Figure 3. (A) Total Hb concentrations ([total Hb]) for different tissue types extracted from diffuse reflectance between 450 and 600 nm. Compared with normal and CIN 1, [total Hb] increased significantly in CIN 2⁺ ($P < .002$). [Total Hb] can also be used to distinguish CIN (CIN 1 + CIN 2⁺) from normal tissue ($P < .023$). (B) Mean reduced scattering coefficient ($\langle \mu_s'(\lambda) \rangle$) from 450 to 600 nm was not significantly decreased in CIN 2⁺ compared with normal and CIN 1, although there was a significant decrease of ($\langle \mu_s'(\lambda) \rangle$) in CIN compared with normal tissue ($P < .002$). Asterisks refer to significance at the $P < .025$ level with the Bonferroni correction.

Table 3. Unpaired Wilcoxon Rank Sum Test Results.

Extracted Parameter	P (450-600 nm)	
	CIN 2 ⁺ (n = 15) vs Normal* + CIN 1 (n = 64)	CIN 1 + CIN 2 ⁺ (n = 33) vs Normal (n = 46)
[oxyHb]	<.001 [†]	.024
[total Hb]	.002	.023
Hb saturation = [oxyHb]/[total Hb]	N/S [‡] (.64)	N/S (.31)
Mean μ_s'	P/S [‡] (.06)	.002

*Normal includes both colposcopically normal and biopsy-confirmed normal.

[†]P < .025 is considered significant with the Bonferroni correction.

[‡]N/S stands for not significant when P ≥ .025; .025 < P < .10 is considered partially significant (P/S).

[27–29]. However, most current technologies are trained to recognize spectral differences between normal and abnormal cervical tissues using empirical techniques and hence cannot be used to quantify the underlying physiological changes associated with dysplastic development. Quantifying the underlying sources of contrast, in our opinion, could lead to streamlined systems that hone in on the physiologic and morphological features that most effectively distinguish high-grade precancers from other tissue types. In addition, our technology can serve as a tool that noninvasively probes the physiological and morphological changes in tissue due to various perturbations such as chemotherapy or radiation therapy, labor, and pathological processes. Using the Monte Carlo–based inverse model, we were able to quantify tissue absorption and scattering, as well as Hb concentration and saturation *in vivo* from diffuse reflectance collected [33,52].

The concentration of oxyHb and total Hb increased significantly (P < .001 and P < .002, respectively) from normal and CIN 1 (grouped together) to CIN 2⁺ (Table 3). However, the concentration of deoxyHb did not show a significant difference between CIN 2⁺ and other tissue types. Therefore, most of the increases in [total Hb] are attributed to increased concentration of oxyHb. From Monte Carlo simulations, the current fiber geometry has an average 75% sensing depth (i.e., the maximum depth that 75% of the detected photons penetrated) equaling to 532 to 868 μm for λ between 450 and 600 nm, well into the cervical stroma. Because most collected photons originate from the vascular stroma, the increase in Hb content in CIN 2⁺ is likely due to angiogenesis, or formation of new blood vessels, that accompanies intraepithelial neoplasia. The concentration of Hb is a direct indicator of tissue vascularity, which may be impacted by angio-

genesis. In contrast to the ovary and the endometrium where angiogenesis plays an important role in normal physiology, angiogenesis in the uterine cervix is involved primarily in neoplastic processes [34]. Multiple groups have confirmed the importance of angiogenesis in the cervical neoplastic development [16,32,35,56,57], independent of the degree of associated inflammation [56].

Using immunohistochemical stains for vascular endothelial cells, Abulafia et al. [34] and Dellas et al. [35] have shown that microvessel density, which is proportional to [total Hb], is positively correlated with cervical precancer grades. Manifestation of neovascularization is along the basement membrane beneath precancerous lesions, indicating that angiogenesis may occur before or concomitant with the transformation to invasive carcinoma. Clinically, this feature may be seen by colposcopy as coarse punctuation or mosaic microvascular patterns on the surface of the cervical precancerous lesion after the application of acetic acid. Neither [oxyHb] nor [total Hb] was significantly different between normal and CIN 1 tissues, suggesting that the increase in vasculature is delayed until more severe dysplastic development as in CIN 2⁺. Smith-McCune et al. [58], using immunohistochemical staining for factor VIII and expression of vascular endothelial growth factor, found no significant difference in angiogenesis between CIN 1 and normal controls yet noted a significant increase in CIN 2⁺ versus normal and in CIN 2⁺ versus CIN 1.

Hemoglobin saturation, defined as the ratio of [oxyHb] to [total Hb], is an indicator of tissue oxygenation, as oxyHb is the dominant oxygen transporter. In our study, no significant differences were observed between the different tissue types, suggesting that oxygenation level is similar in normal and precancerous tissues in the sensing depth of our probe. Using immunohistochemical staining on cervical biopsies, Lee et al. [59] showed that hypoxia-inducible factor 1α activity was highly expressed in normal, CIN 1, and CIN 2 but decreased significantly in CIN 3. Because hypoxia-inducible factor 1α expression was confined to the hypoxic basal epithelial cells (and later throughout the epithelium with increasing severity), the primarily stromal-sensing depth of the probe may have prevented the detection of the contrast in Hb saturation.

Using diffuse reflectance data from 450 to 600 nm, mean reduced scattering decreased significantly from normal to precancerous tissues (P < .002) in our study. Although epithelial scattering is expected to increase with dysplastic transformation of the epithelial cells [60], stromal scattering has been shown to decrease due to the breakdown

Table 4. Comparison of Physiological and Optical Properties Measured from the Cervix *In Vivo*.

Technique	Reference	λ (nm)	Normal (Mean ± SE)				CIN 2 ⁺ (Mean ± SE)			
			n	[Total Hb] (μM)	Hb Saturation (%)	μ_s' (cm ⁻¹)	N	[Total Hb] (μM)	Hb Saturation (%)	μ_s' (cm ⁻¹)
Diffuse reflectance spectroscopy	This paper	450-600	40	7.90 ± 1.03	95.3 ± 3.3	12.41 ± 0.72	11	16.24 ± 5.93	94.3 ± 4.5	8.62 ± 1.00
Near IR spectroscopy	[16]	674, 811, 849, 956	10	124.7 ± 7.1 ^{†‡}	84.9 ± 1.1	9.05 ± 0.48 (674 nm)	10	88.6 ± 11.3 (* P < .0022)	76.5 ± 4.6 (P < .0786)	4.98 ± 0.11 (674 nm) (P < .161)
Diffuse reflectance spectroscopy	[11]	350-700	55	N/A	N/A	30 (squamous metaplasia, 475 nm)	11	N/A	N/A	18 (475 nm)
Polarized light scattering	[32]	500-1000	77 [§]	0.9 ± 0.2 ^{†,*,§}	5.1 ± 0.3 [†]	N/A	11	1.8 ± 0.9 (P < .106)	6.1 ± 0.6 (P < .168)	N/A

*Indicates significance (at P < .05) difference between normal and CIN 2⁺.

[†]Reported standard deviation (SD) were converted to SE for easier comparison (SE = SD/√n).

[‡]Primarily stromal absorption because estimated sensing depth is 3 mm.

[§]Includes 59 normal (50 colposcopically normal + 9 biopsy-confirmed normal), 8 cervicitis, and 10 CIN 1.

[¶]No units were given for these values.

of collagen. Several groups [12,19,45] have observed a decrease in collagen fluorescence in CIN compared with colposcopically normal tissue. Because collagen is a major scatterer in the visible wavelength, stromal scattering is expected to decrease in CIN compared with normal tissue. Considering that the sensing depth of our probe is primarily in the stroma, decreased stromal scattering causes observed scattering to decrease overall with severity of precancerous lesion. Georgakoudi et al. [11] also observed a similar decrease in scattering from metaplastic to CIN 2⁺ using diffuse reflectance spectroscopy. Mean reduced scattering did not decrease significantly when normal and CIN 1 were combined *versus* CIN 2⁺ ($P < .06$), although dysplastic cervix (CIN) has a significantly lower scattering compared with normal tissue ($P < .002$), suggesting that destruction of collagen fibers is most significant upon the initial neoplastic development (as in CIN 1) and does not decrease significantly between CIN 1 and CIN 2⁺.

Results of quantitative optical studies of the cervix are summarized in Table 4. CIN 1 was excluded from Table 4 because not all studies included this category. Hornung et al. [16] quantified higher [total Hb] than what we have reported in our study, which is likely due to a significantly greater volume weighting of the stroma with an estimated sensing depth of 3 mm. Because [total Hb] is expected to increase with angiogenesis, the decrease in [total Hb] from normal to CIN 2⁺ by Hornung et al. [16] is likely due to other biochemical changes or modeling assumptions. Mourant et al. [32], using polarized elastic light scattering from 500 to 1000 nm, did not observe a statistically different [total Hb] between CIN 2⁺ and normal, CIN 1, and cervicitis tissues. Hemoglobin saturation values reported in the studies by Hornung et al. [16] and Mourant et al. [32] were similar to ours and drew similar conclusions in that no significant differences in Hb saturation were observed between normal and high-grade precancerous tissues.

We have assessed the capability of our diffuse reflectance system and inverse model to characterize optical and physiological parameters of normal and dysplastic cervical tissues. Despite interpatient variability from fluctuations in normal physiology, statistically significant differences were observed in [total Hb] ($P < .002$) and mean reduced scattering (partially significant at $P < .06$) in CIN 2⁺ *versus* normal and CIN 1, clinically the most important classification to avoid overtreatment. Ratios of extracted parameters may also be used to classify different tissue types, especially when changes of opposite directions are combined into one ratio to increase statistical power. For instance, the statistical power in discriminating normal and CIN 1 from CIN 2⁺ was improved when the ratio of [total Hb] over mean $\mu_s'(\lambda)$ was used. The ability to quantify physiological and morphological changes is useful not only in the diagnosis of cervical precancers but also in the planning and monitoring of therapies. Moreover, quantification of physiological parameters may allow correlation with angiogenesis and other tissue parameters to provide insights into tissue carcinogenesis. Future improvements to increase the sample size as well as using an oblique fiber optimized for detecting layer-dependent optical contrasts are underway.

Acknowledgments

The authors thank all the patients who have participated in this study, as well as the staff at Duke University Medical Center Colposcopy Clinic. The authors are grateful for the statistical guidance provided by William Barry.

References

- [1] NCI (2008). *Surveillance Epidemiology and End Results (SEER)*. Bethesda, MD: National Cancer Institute.
- [2] Wright TC, Kurman RJ, and Ferenczy A (1994). Cervical intraepithelial neoplasia. In A Blaustein (Ed.). *Pathology of the Female Genital Tract*. New York, NY: Springer-Verlag.
- [3] Guido R, Schiffman M, Solomon D, and Burke L (2003). Postcolposcopy management strategies for women referred with low-grade squamous intraepithelial lesions or human papillomavirus DNA-positive atypical squamous cells of undetermined significance: a two-year prospective study. *Am J Obstet Gynecol* **188** (6), 1401–1405.
- [4] Mitchell MF, Schottenfeld D, Tortolero-Luna G, Cantor SB, and Richards-Kortum R (1998). Colposcopy for the diagnosis of squamous intraepithelial lesions: a meta-analysis. *Obstet Gynecol* **91** (4), 626–631.
- [5] Ferlay J, Bray F, Pisani P, and Parkin DM (2004). *GLOBOCAN 2002: Cancer Incidence, Mortality and Prevalence Worldwide*. Lyon, France: IARC Press.
- [6] Balas CJ, Themelis GC, Prokopakis EP, Orfanoudaki I, Koumantakis E, and Helidonis ES (1999). *In vivo* detection and staging of epithelial dysplasias and malignancies based on the quantitative assessment of acetic acid–tissue interaction kinetics. *J Photochem Photobiol B* **53** (1–3), 153–157.
- [7] Monsonego J, Bosch FX, Coursaget PJ, Cox T, Franco E, Frazer I, Sankaranarayanan R, Schiller J, Singer A, Wright T, et al. (2004). Cervical cancer control, priorities and new directions. *Int J Cancer* **108** (3), 329–333.
- [8] Wright TC Jr (2003). Chapter 10: cervical cancer screening using visualization techniques. *J Natl Cancer Inst Monogr* **2003** (31), 66–71.
- [9] Arifler D, MacAulay C, Follen M, and Richards-Kortum R (2006). Spatially resolved reflectance spectroscopy for diagnosis of cervical precancer: Monte Carlo modeling and comparison to clinical measurements. *J Biomed Opt* **11** (6), 064027-16.
- [10] Chang SK, Mirabal YN, Atkinson EN, Cox D, Malpica A, Follen M, and Richards-Kortum R (2005). Combined reflectance and fluorescence spectroscopy for *in vivo* detection of cervical pre-cancer. *J Biomed Opt* **10** (2), 024031-11.
- [11] Georgakoudi I, Sheets EE, Müller MG, Backman V, Crum CP, Badizadegan K, Dasari RR, and Feld MS (2002). Trimodal spectroscopy for the detection and characterization of cervical precancers *in vivo*. *Am J Obstet Gynecol* **186** (3), 374–382.
- [12] Pavlova I, Sokolov K, Drezek R, Malpica A, Follen M, and Richards-Kortum R (2003). Microanatomical and biochemical origins of normal and precancerous cervical autofluorescence using laser-scanning fluorescence confocal microscopy. *Photochem Photobiol* **77**, 550–555.
- [13] Balas C (2001). A novel optical imaging method for the early detection, quantitative grading, and mapping of cancerous and precancerous lesions of cervix. *IEEE Trans Biomed Eng* **48** (1), 96–104.
- [14] Pogue BW, Mycek MA, and Harper D (2000). Image analysis for discrimination of cervical neoplasia. *J Biomed Opt* **5** (1), 72–82.
- [15] Georgakoudi I, Sheets EE, Crum CP, Mueller MG, Backman V, and Feld MS (2001). Tri-modal spectroscopy as a tool for detecting cervical squamous intraepithelial lesions *in vivo*. In T Papazoglou and GA Wagnieres (Chair). *Diagnostic Optical Spectroscopy in Biomedicine, Munich, Germany, 17 June 2001. Proc. SPIE* **4432**, 1–9.
- [16] Hornung R, Pham TH, Keefe KA, Berns MW, Tadir Y, and Tromberg BJ (1999). Quantitative near-infrared spectroscopy of cervical dysplasia *in vivo*. *Hum Reprod* **14** (11), 2908–2916.
- [17] Mirabal YN, Chang SK, Atkinson EN, Malpica A, Follen M, and Richards-Kortum R (2002). Reflectance spectroscopy for *in vivo* detection of cervical precancer. *J Biomed Opt* **7** (4), 587–594.
- [18] Orfanoudaki IM, Themelis GC, Sifakis SK, Fragouli DH, Panayiotides JG, Vazgiouraki EM, and Koumantakis EE (2005). A clinical study of optical biopsy of the uterine cervix using a multispectral imaging system. *Gynecol Oncol* **96** (1), 119–131.
- [19] Ramanujam N, Mitchell MF, Mahadevan A, Warren S, Thomsen S, Silva E, and Richards-Kortum R (1994). *In vivo* diagnosis of cervical intraepithelial neoplasia using 337-nm-excited laser-induced fluorescence. *Proc Natl Acad Sci USA* **91** (21), 10193–10197.
- [20] Sokolov K, Follen M, and Richards-Kortum R (2002). Optical spectroscopy for detection of neoplasia. *Curr Opin Chem Biol* **6** (5), 651–658.
- [21] Shah N, Cerussi A, Eker C, Espinoza J, Butler J, Fishkin J, Hornung R, and Tromberg B (2001). Noninvasive functional optical spectroscopy of human breast tissue. *Proc Natl Acad Sci USA* **98** (8), 4420–4425.
- [22] Volynskaya Z, Haka AS, Bechtel KL, Fitzmaurice M, Shenk R, Wang N, Nazemi J, Dasari RR, and Feld MS (2008). Diagnosing breast cancer using

- diffuse reflectance spectroscopy and intrinsic fluorescence spectroscopy. *J Biomed Opt* **13** (2), 024012.
- [23] Zhu C, Palmer GM, Breslin TM, Xu F, and Ramanujam N (2005). Use of a multiseparation fiber optic probe for the optical diagnosis of breast cancer. *J Biomed Opt* **10** (2), 024032.
- [24] DaCosta RS, Wilson BC, and Marcon NE (2005). Optical techniques for the endoscopic detection of dysplastic colonic lesions. *Curr Opin Gastroenterol* **21** (1), 70–79.
- [25] Dhar A, Johnson KS, Novelli MR, Bown SG, Bigio IJ, Lovat LB, and Bloom SL (2006). Elastic scattering spectroscopy for the diagnosis of colonic lesions: initial results of a novel optical biopsy technique. *Gastrointest Endosc* **63** (2), 257–261.
- [26] Nieman LT, Kan C-W, Gillenwater A, Markey MK, and Sokolov K (2008). Probing local tissue changes in the oral cavity for early detection of cancer using oblique polarized reflectance spectroscopy: a pilot clinical trial. *J Biomed Opt* **13** (2), 024011.
- [27] Alvarez R and Wright T (2007). Effective cervical neoplasia detection with a novel optical detection system: a randomized trial. *Gynecol Oncol* **104** (2), 281–289.
- [28] Cardenas-Turanzas M, Freeberg JA, Benedet JL, Atkinson EN, Cox DD, Richards-Kortum R, MacAulay C, Follen M, and Cantor SB (2007). The clinical effectiveness of optical spectroscopy for the *in vivo* diagnosis of cervical intraepithelial neoplasia: where are we? *Gynecol Oncol* **107** (1, Suppl 1), S138–S146.
- [29] Schomacker KT, Meese TM, Jiang C, Abele CC, Dickson K, Sum ST, and Flewelling RF (2006). Novel optical detection system for *in vivo* identification and localization of cervical intraepithelial neoplasia. *J Biomed Opt* **11** (3), 034009–034012.
- [30] Zuluaga AF, Follen M, Boiko I, Malpica A, and Richards-Kortum R (2005). Optical coherence tomography: a pilot study of a new imaging technique for noninvasive examination of cervical tissue. *Am J Obstet Gynecol* **193** (1), 83–88.
- [31] Collier T, Arifler D, Malpica A, Follen M, and Richards-Kortum R (2003). Determination of epithelial tissue scattering coefficient using confocal microscopy. *IEEE J Sel Top Quantum Electron* **9** (2), 307–313.
- [32] Mourant JR, Bocklage TJ, Powers TM, Greene HM, Bullock KL, Marr-Lyon LR, Dorin MH, Waxman AG, Zsemlye MM, and Smith HO (2007). *In vivo* light scattering measurements for detection of precancerous conditions of the cervix. *Gynecol Oncol* **105** (2), 439–445.
- [33] Palmer G and Ramanujam N (2006). Monte Carlo–based inverse model for calculating tissue optical properties. Part I: Theory and validation on synthetic phantoms. *Appl Opt* **45** (5), 1062–1071.
- [34] Abulafia O and Sherer D (2000). Angiogenesis in the uterine cervix. *Int J Gynecol Cancer* **10** (5), 349.
- [35] Dellas A, Moch H, Schultheiss E, Feichter G, Almendral AC, Gudat F, and Torhorst J (1997). Angiogenesis in cervical neoplasia: microvessel quantitation in precancerous lesions and invasive carcinomas with clinicopathological correlations. *Gynecol Oncol* **67** (1), 27–33.
- [36] Lee J, Kim H, Jung J, Lee M, and Park C (2002). Angiogenesis, cell proliferation and apoptosis in progression of cervical neoplasia. *Anal Quant Cytol Histol* **24** (2), 103–113.
- [37] Obermair A, Bancher-Todesca D, Bilgi S, Kaider A, Kohlberger P, Mullauer-Ertl S, Leodolter S, and Gitsch G (1997). Correlation of vascular endothelial growth factor expression and microvessel density in cervical intraepithelial neoplasia. *J Natl Cancer Inst* **89** (16), 1212–1217.
- [38] Ravazoula P, Zolota V, Hatjicondi O, Sakellaropoulos G, Kourounis G, and Maragoudakis ME (1996). Assessment of angiogenesis in human cervical lesions. *Anticancer Res* **16** (6B), 3861–3864.
- [39] Zhu C, Palmer GM, Breslin TM, Xu F, and Ramanujam N (2005). Use of a multiseparation fiber optic probe for the optical diagnosis of breast cancer. *J Biomed Opt* **10** (2), 024032.
- [40] Zhu C, Palmer GM, Breslin TM, Harter J, and Ramanujam N (2006). Diagnosis of breast cancer using diffuse reflectance spectroscopy: comparison of a Monte Carlo *versus* partial least squares analysis based feature extraction technique. *Lasers Surg Med* **38** (7), 714–724.
- [41] Liu Q, Zhu C, and Ramanujam N (2003). Experimental validation of Monte Carlo modeling of fluorescence in tissues in the UV-visible spectrum. *J Biomed Opt* **8** (2), 223–236.
- [42] Wang L, Jacques SL, and Zheng L (1995). MCML—Monte Carlo modeling of light transport in multi-layered tissues. *Comput Methods Programs Biomed* **47** (2), 131–146.
- [43] Chang SK, Arifler D, Drezek R, Follen M, and Richards-Kortum R (2004). Analytical model to describe fluorescence spectra of normal and preneoplastic epithelial tissue: comparison with Monte Carlo simulations and clinical measurements. *J Biomed Opt* **9** (3), 511–522.
- [44] Walker DC, Brown BH, Blackett AD, Tidy J, and Smallwood RH (2003). A study of the morphological parameters of cervical squamous epithelium. *Physiol Meas* **24** (1), 121–135.
- [45] Drezek R, Sokolov K, Utzinger U, Boiko I, Malpica A, Follen M, and Richards-Kortum R (2001). Understanding the contributions of NADH and collagen to cervical tissue fluorescence spectra: modeling, measurements, and implications. *J Biomed Opt* **6** (4), 385–396.
- [46] Wright TC Jr, Massad LS, Dunton CJ, Spitzer M, Wilkinson EJ, and Solomon D (2007). 2006 consensus guidelines for the management of women with abnormal cervical cancer screening tests. *Am J Obstet Gynecol* **197** (4), 346–355.
- [47] Wright TC Jr, Massad LS, Dunton CJ, Spitzer M, Wilkinson EJ, and Solomon D (2007). 2006 consensus guidelines for the management of women with cervical intraepithelial neoplasia or adenocarcinoma *in situ*. *Am J Obstet Gynecol* **197** (4), 340–345.
- [48] Moscicki A-B (2005). Human papilloma virus, Papanicolaou smears, and the college female. *Pediatr Clin North Am* **52** (1), 163–177.
- [49] Prah S. Tabulated molar extinction coefficient for hemoglobin in water. <http://omlc.org.edu/spectra/hemoglobin/summary.html>. Accessed on September 10, 2008.
- [50] Bender JE, Vishwanath K, Moore LK, Brown JQ, Chang V, Palmer GM, and Ramanujam N (in press). A robust Monte Carlo model for the extraction of biological absorption and scattering *in vivo*. *IEEE Trans Biomed Eng*. Accessed online at <http://xplqa.ieee.org/xpl/tocpreprint.jsp?jnumber=4359967&Submit3=View+Articles&pnumber=10>.
- [51] Liu Q (2006). Sequential estimation of optical properties of a two-layered epithelial tissue model from depth-resolved ultraviolet-visible diffuse reflectance spectra. *Appl Opt* **45** (19), 4776.
- [52] Palmer GM, Zhu C, Breslin TM, Xu F, Gilchrist KW, and Ramanujam N (2006). Monte Carlo–based inverse model for calculating tissue optical properties. Part II: Application to breast cancer diagnosis. *Appl Opt* **45** (5), 1072–1078.
- [53] Skala MC, Palmer GM, Vrotsos KM, Gendron-Fitzpatrick A, and Ramanujam N (2007). Comparison of a physical model and principal component analysis for the diagnosis of epithelial neoplasias *in vivo* using diffuse reflectance spectroscopy. *Opt Express* **15** (12), 7863–7875.
- [54] Yu B, Fu H, Bydlon T, Bender JE, and Ramanujam N (2008). Diffuse reflectance spectroscopy with a self-calibrating fiber optic probe. *Opt Lett* **33** (16), 1783–1785.
- [55] Zhu C, Palmer GM, Breslin TM, Harter J, and Ramanujam N (2008). Diagnosis of breast cancer using fluorescence and diffuse reflectance spectroscopy: a Monte-Carlo-model–based approach. *J Biomed Opt* **13** (3), 034015-15.
- [56] Burton JL and Wells M (2001). Angiogenesis in gynaecological cancer. *CME J Gynecol Oncol* **5** (2), 156–163.
- [57] Vieira SC, Zeferino LC, da Silva BB, Aparecida Pinto G, Vassallo J, Carasan GAF, and de Moraes NG (2004). Quantification of angiogenesis in cervical cancer: a comparison among three endothelial cell markers. *Gynecol Oncol* **93** (1), 121–124.
- [58] Smith-McCune KK and Weidner N (1994). Demonstration and characterization of the angiogenic properties of cervical dysplasia. *Cancer Res* **54** (3), 800–804.
- [59] Lee W-Y, Huang S-C, Hsu K-F, Tzeng C-C, and Shen W-L (2008). Roles for hypoxia-regulated genes during cervical carcinogenesis: somatic evolution during the hypoxia-glycolysis-acidosis sequence. *Gynecol Oncol* **108** (2), 377–384.
- [60] Collier T (2005). Sources of scattering in cervical tissue: determination of the scattering coefficient by confocal microscopy. *Appl Opt* **44** (11), 2072.